bioRxiv preprint doi: https://doi.org/10.1101/2021.08.18.456762; this version posted August 18, 2021. The copyright holder for this preprint (which was not certified by peer review) is the author/funder. All rights reserved. No reuse allowed without permission.

DNA Origami Voltage Sensors for Transmembrane Potentials with Single-Molecule Sensitivity

Sarah E. Ochmann[†], Himanshu Joshi[‡], Ece Büber[†], Henri G. Franquelim[§], Pierre Stegemann[⊥], Barbara Saccà[⊥], Ulrich F. Keyser[‖], Aleksei Aksimentiev[‡], Philip Tinnefeld[,†]*

[†]Department of Chemistry and Center for NanoScience, Ludwig-Maximilians-Universität München, 81377 München, Germany

[‡]Department of Physics and Beckman Institute for Advanced Science and Technology, University of Illinois, Urbana, Illinois 61820, United States

[§]Max Planck Institute of Biochemistry, 82152 Planegg, Germany

[⊥]Center of Medical Biotechnology (ZMB) and Center for Nano Integration Duisburg-Essen (CENIDE), University of Duisburg-Essen, 45117 Essen, Germany

[‖]Cavendish Laboratory, Department of Physics, University of Cambridge, JJ Thomson Avenue, Cambridge, CB3 0HE, United Kingdom

KEYWORDS. DNA origami, voltage sensor, single-molecule FRET, transmembrane potential, voltage imaging, molecular dynamic simulations

ABSTRACT**.** Signal transmission in neurons goes along with changes in the transmembrane potential. To report them, different approaches including optical voltage-sensing dyes and genetically encoded voltage indicators have evolved. Here, we present a DNA nanotechnology-based system. Using DNA origami,

bioRxiv preprint doi: https://doi.org/10.1101/2021.08.18.456762; this version posted August 18, 2021. The copyright holder for this preprint (which was not certified by peer review) is the author/funder. All rights reserved. No reuse allowed without permission.

we incorporate and optimize different properties such as membrane targeting and voltage sensing modularly. As a sensing unit, we use a hydrophobic red dye anchored to the membrane and an anionic green dye at the DNA connecting the DNA origami and the membrane dye anchor. Voltage-induced displacement of the anionic donor unit is read out by changes of Fluorescence Resonance Energy Transfer (FRET) of single sensors attached to liposomes. They show a FRET change of ~5% for $\Delta\Psi$=100 mV and allow adapting the potential range of highest sensitivity. Further, the working mechanism is rationalized by molecular dynamics simulations. Our approach holds potential for the application as non-genetically encoded sensors at membranes.

INTRODUCTION. The electrical transmembrane potential $\Delta\Psi$ on the cellular level is a key parameter in the neurosciences. The introduction of fluorescence-based voltage sensors was a milestone towards a broader application and non-invasive visualization approaches in contrast to electrophysiological approaches being invasive, serial and time consuming.[1] Many challenges with respect to signal, contrast and response time have been addressed with Genetically Encoded Voltage Indicators (GEVIs)[2–4] that offer targetability to cell membranes. For improved contrast and imaging durations, hybrid approaches combining GEVIs with organic fluorophores have been introduced.[5,6] These approaches, however, require transfected cell lines or transgenic animals.

In contrast, conventional voltage-sensing dyes face the challenge that all functionalities including targeting membranes, sensing and transducing a signal, have to be encoded in simple, chemically accessible structures. The development of a first generation of sensors yielded low-contrast Stark-effect voltage-sensing dyes and probes that disturbed cellular functions e.g. by capacitive loading of the membrane.[7] Therefore, in recent approaches the complexity of sensors has been increased including bottom-up nanotechnological ideas to develop e.g. quantum-confined semiconductor nanoparticles or quantum dot-fullerene bioconjugates for voltage sensing.[8–10] Recently, DNA was used as scaffolding material to combine electron-transfer based voltage-sensing dyes[7,11,12] with targeting and intensity referencing for voltage sensing in organelles.[13]

bioRxiv preprint doi: https://doi.org/10.1101/2021.08.18.456762; this version posted August 18, 2021. The copyright holder for this preprint (which was not certified by peer review) is the author/funder. All rights reserved. No reuse allowed without permission.

Here, we use DNA origami to modularly address different challenges of voltage sensor design and demonstrate an alternative voltage-sensing strategy that allows sensing with bright dyes compatible with single-molecule imaging. DNA origami and similar self-assembly techniques offer the potential to meet the broad demands such as targeting lipid membranes, incorporating a sensing unit, providing a transduction mechanism optionally with internal referencing, being bio-compatible and minimally invasive.

In the DNA origami method, a long single-stranded DNA molecule (ssDNA, >7000 nucleotides long) is folded into a desired shape by hybridization with short oligonucleotides, producing billions of identical nanostructures.[14–16] This bottom-up nanoassembly method offers the ability to place any chemical moiety by the integration of modified oligonucleotides on the nanostructure like on a molecular breadboard. Using the DNA origami technique, a variety of sensors has been realized,[17] from nanopores[18–20] to drug delivery systems[21,22] to force sensors.[23,24] By capturing DNA origami on nanocapillary tips, Hemmig and Fitzgerald *et al.* demonstrated the feasibility of using a DNA origami construct as a single-molecule voltage sensor.[25] Two fluorophores capable of interacting *via* Fluorescence Resonance Energy Transfer (FRET) are placed on a DNA nanostructure such that, when subject to a voltage bias at the tip of a nanopipet, the FRET efficiency is modulated by the voltage magnitude.

Here, we demonstrate single-molecule transmembrane voltage read-out from the surface of a lipid membrane. By using a rectangular DNA origami for the arrangement of the different components needed, we create a sensor that optically reads out defined potentials via FRET with a change of ~5% for $\Delta\Psi$=100 mV. FRET offers an advantageous ratiometric signal read-out and is therefore signal-intensity independent. We detect single FRET pairs by spacing out origami structures beyond the diffraction limit and hence, provide a pathway to image at the nanoscale beyond ensemble averages. We rationalize the functioning of the sensor through molecular dynamics (MD) simulations of the DNA-lipid membrane assembly. Further, we demonstrate the potential of DNA nanotechnology for voltage sensing by

bioRxiv preprint doi: https://doi.org/10.1101/2021.08.18.456762; this version posted August 18, 2021. The copyright holder for this preprint (which was not certified by peer review) is the author/funder. All rights reserved. No reuse allowed without permission.

introducing small molecular changes in the sensing unit to shift the sensitivity of the sensor towards negative $\Delta\Psi$.

RESULTS**.** The transmembrane voltage sensor is based on a rectangular DNA origami with dimensions of 70x100 nm[14,26,27] functioning as a platform to program all the functionalities required into a small entity. In order to bind to liposomes, the nanostructure is equipped with ten cholesterol moieties and for binding to biotinylated PLL-e-PEG passivated surfaces, additional six biotin moieties are incorporated (Figure 1a, S1 and Table S1). Surface binding of the liposomes via the DNA origami facilitates imaging by total internal reflection microscopy (TIRF) while avoiding direct surface interactions of the liposomes.[28] The voltage-sensing unit is placed centrally on the platform protruding from the structure. The hydrophobic and cationic dye ATTO647N connected to DNA by a C_{12}-phosphate-C_6 chain (C_{12}+C_6) is expected to anchor the sensor unit in the lipid membrane (Figure 1b and Figure S2 for molecular structures). Insertion into the lipid core of the membrane was observed for ATTO647N before.[29] The DNA connection from ATTO647N to the DNA origami platform contains the anionic fluorophore ATTO532. We reason that any change of potential should have opposite effects on the average positions of the cationic ATTO647N dye and the anionic ATTO532 dye on the anionic DNA linker. The opposite forces on the two dyes should translate a $\Delta\Psi$ into a change of FRET that can be read out optically and on the level of single molecules.

bioRxiv preprint doi: https://doi.org/10.1101/2021.08.18.456762; this version posted August 18, 2021. The copyright holder for this preprint (which was not certified by peer review) is the author/funder. All rights reserved. No reuse allowed without permission.

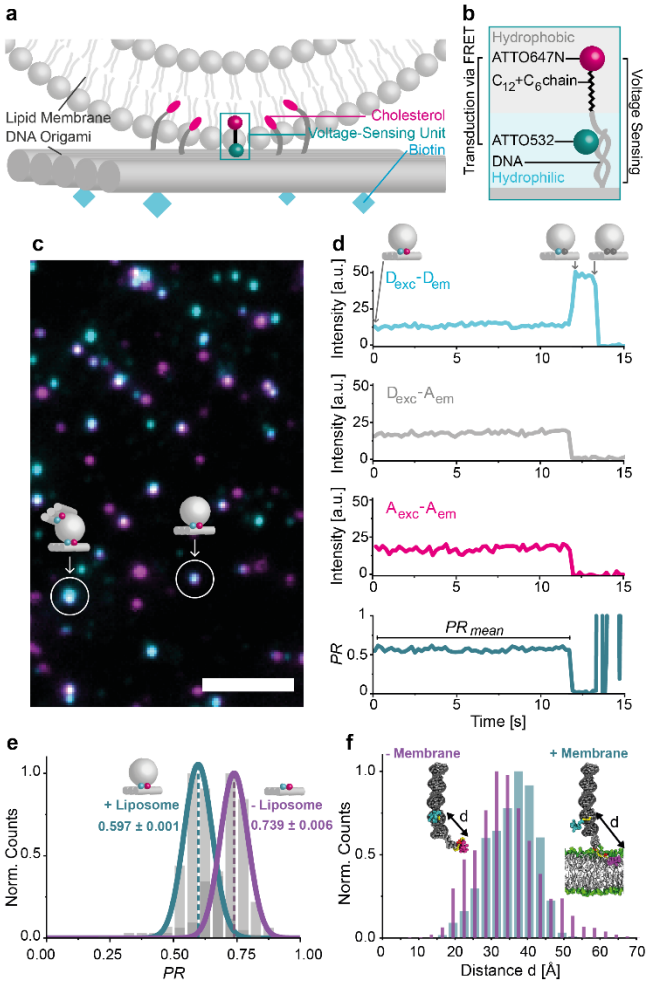

Figure 1. (a) DNA origami sensor of transmembrane potentials. A rectangular DNA origami plate is decorated with cholesterols to bind a liposome and with biotins to attach to the neutravidin-functionalized surface of a microscope's cover slip. The voltage-sensing unit is positioned in the center of the DNA origami. (b) Voltage-sensing unit consisting of dsDNA protruding from the DNA origami plate and carrying an ATTO532 dye, and a complementary strand with an ATTO647N dye connected *via* a C_{12}+C_6 linker (see Figure S2 for chemical structure). The transduction of voltage signal to fluorescence is fulfilled by FRET from the donor ATTO532 to the acceptor ATTO647N. (c) Superimposed TIRF image of donor (blue) and acceptor (pink) fluorescence from DNA origami. White spots indicate DNA origami plates with both donor and acceptor dyes. The scale bar refers to 5 µm. (d) Single-molecule FRET transient. The fluorescence intensity over time is shown for the donor excitation-donor emission D_{exc}-D_{em} channel (light blue), the donor excitation-acceptor emission D_{exc}-A_{em} channel (grey) and the acceptor excitation-

bioRxiv preprint doi: https://doi.org/10.1101/2021.08.18.456762; this version posted August 18, 2021. The copyright holder for this preprint (which was not certified by peer review) is the author/funder. All rights reserved. No reuse allowed without permission.

acceptor emission A_{exc}-A_{em} channel (pink). From the D_{exc}-D_{em} and the D_{exc}-A_{em} channels, the *Proximity Ratio PR* and the PR_{mean} is determined (dark blue). (e) *PR* distributions for DNA origami constructs with (cyan) and without (purple) liposome attachment. The error refers to the standard error of the mean. $N_{molecule}$ is ≥100 for each sample. (f) Histogram of inter-dye distances obtained from MD simulations of a dsDNA duplex decorated with the two dyes positioned at the lipid-water interface (cyan) and in aqueous solution (purple). Simulation times: - Membrane 1.35 µs, + Membrane 1.55 µs.

For imaging, we perform single-molecule FRET (smFRET) experiments[30] of the optical potential sensor on a homebuilt TIRF microscope with green-red alternating laser excitation (ALEx, for details see SI).[31,32] We acquire videos to follow the fluorescence over time and verify that single DNA origamis are observed. Figure 1c presents a superimposed TIRF image with donor dyes in cyan, acceptor dyes in pink and an overlay of the two in white. Some of the spots are brighter than others which is caused by multiple DNA origamis bound to a single liposome or origami multimers. To eliminate such aggregates in further analysis, we generate intensity-time transients from the videos for each spot with the software iSMS[33] and inspect them visually. An exemplary transient is shown in Figure 1d with D_{exc}-D_{em} (light blue), D_{exc}-A_{em} (grey) and A_{exc}-A_{em} (pink) with the subscript indicating the excitation and emission channels of donor (D) and acceptor (A), respectively. A correlated intensity increase in D_{exc}-D_{em} upon an intensity decrease in D_{exc}-A_{em} and A_{exc}-A_{em} as well as a rapid photobleaching in D_{exc}-D_{em} are a clear indication that indeed a single DNA origami is observed. From the intensities I_{DD} of the D_{exc}-D_{em} and the intensity I_{DA} of the D_{exc}-A_{em} channel, FRET is quantified as the *Proximity Ratio PR* with

$$PR = \frac{I_{DA}}{I_{DD}+I_{DA}} \quad (1)$$

The PR_{mean} is calculated over the whole period of the energy transfer (bottom transient in Figure 1d) yielding one data point for each voltage sensor. All single-molecule transients are carefully reviewed and the ones showing a clear correlation between the three channels mentioned above are picked whereas transients showing multi-chromophore behavior are rejected.

bioRxiv preprint doi: https://doi.org/10.1101/2021.08.18.456762; this version posted August 18, 2021. The copyright holder for this preprint (which was not certified by peer review) is the author/funder. All rights reserved. No reuse allowed without permission.

We first test whether an interaction between the voltage sensor and the lipid membrane as intended is detected. To this end, we study the DNA origamis with and without 100 nm DOPC liposomes by mixing the origami structures with an excess of liposomes and immobilizing the complexes on a surface. After performing smFRET measurements, we obtain *PR* distributions as shown in Figure 1e. The liposome-free sample yields a mean *PR* of 0.739±0.006 (standard error of the mean, SEM) obtained from Gaussian fitting of the distribution which decreases to 0.597±0.001 for the liposome-containing sample (Figure 1e). The fact that we obtain narrow homogenous populations that are clearly shifted with respect to each other indicates quantitative binding of DNA origami voltage sensors to the liposomes. In addition, the decrease of FRET supports the idea that the hydrophobic ATTO647N is diving into the membrane core so that the average distance of donor and acceptor is substantially increased upon membrane binding.

We further rationalize the idea of the FRET-acceptor anchoring in the membrane by MD simulations of the voltage-sensing unit with and without a lipid membrane present (Figure 1f and S3). The Movie S1 provided in the SI reveals a coiling of the ATTO647N with the alkyl chain resulting in a close proximity of the dyes. This secondary structure is broken in the presence of a lipid membrane (Movie S2) as ATTO647N and the alkyl chain insert to and remain in the hydrophobic core of the membrane. Figure 1f shows the distributions for the inter-dye distances for both samples determined from the MD simulations. The observed shift towards larger distances for the sensor in presence of a membrane is in good agreement with the experimental results (Figure 1e) and suggests that the lower *PR* upon liposome addition is a result of the spatial separation of the two dyes. Another interesting observation from the simulations is that the ATTO647N dye remains embedded in the nearest to the membrane, interacting with the phosphate moieties of the lipid head groups (likely because of its positive charge) while the main body of the dye resides inside the hydrophobic core of the membrane.

In order to test the performance of our voltage-sensing DNA origami, we use ion exchange by the ionophore valinomycin[34] to create a well-defined drop of $\Delta\Psi$ across the liposome membrane. In a typical experiment, the origami-liposome complexes are imaged, the buffer surrounding is exchanged to

bioRxiv preprint doi: https://doi.org/10.1101/2021.08.18.456762; this version posted August 18, 2021. The copyright holder for this preprint (which was not certified by peer review) is the author/funder. All rights reserved. No reuse allowed without permission.

introduce a potassium gradient across the lipid membrane and valinomycin is added, before the sample is imaged again (Figure 2a). Valinomycin specifically complexes potassium but not sodium ions and shuttles them across the lipid membrane until an equilibrium is reached and a polarized membrane results following the Nernst equation

$$\Delta\Psi = \frac{RT}{Fz} \ln\left(\frac{c_{in}^{K^+}}{c_{out}^{K^+}}\right) \tag{2}$$

where R is the gas constant, T is the temperature, F is the Faraday constant, z is the charge number and $c_{in}^{K^+}$ and $c_{out}^{K^+}$ are the potassium concentrations inside and outside of the liposome, respectively. By adjusting the initial K^+ concentration gradient, we produce well-defined ΔΨ (Table S2). Figure S4 confirms the functionality of our assay in bulk experiments using a commercially available voltage-sensing dye.

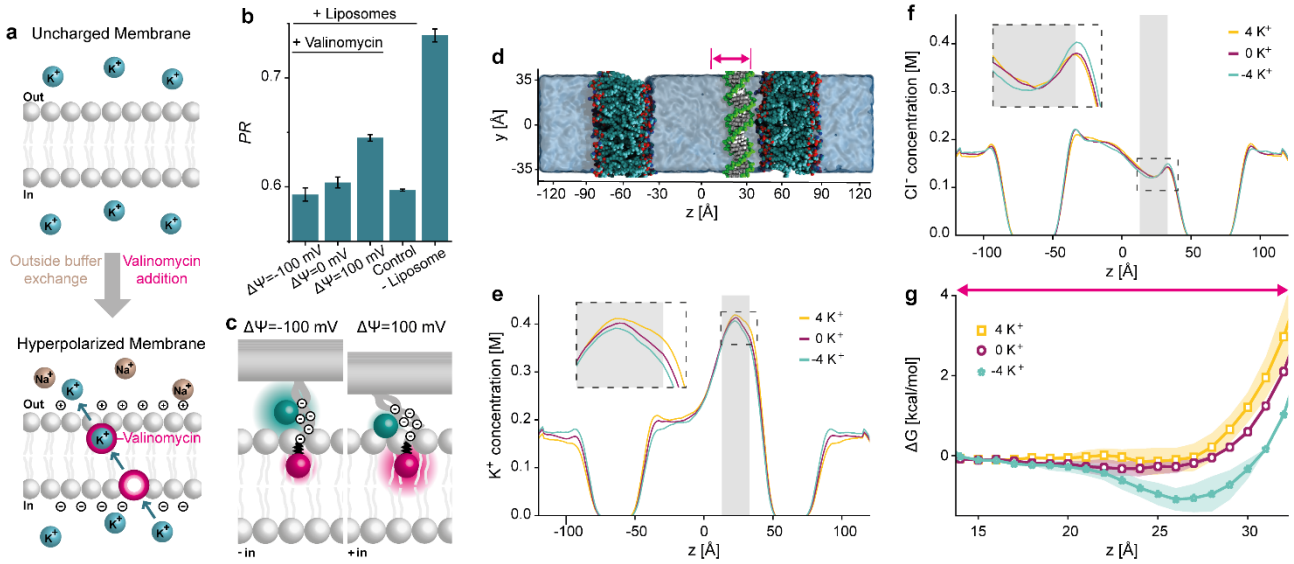

Figure 2. (a) Creation of electrical transmembrane potentials ΔΨ. By exchanging the outside buffer, a potassium ion gradient across the lipid membrane is built up. Equilibration of the potassium gradient by the ionophore valinomycin converts the chemical potential into an electrical transmembrane potential ΔΨ. (b) Mean *PR* and standard errors of the mean derived from Gauss fits to the distributions (Figure S5 and S6) of the DNA origami-liposome complexes with different ΔΨ in comparison to control samples presented in Figure 1e. N_{molecule} is ≥100 for each sample. (c) Proposed working principle of voltage-

bioRxiv preprint doi: https://doi.org/10.1101/2021.08.18.456762; this version posted August 18, 2021. The copyright holder for this preprint (which was not certified by peer review) is the author/funder. All rights reserved. No reuse allowed without permission.

sensing DNA origami. The ATTO647N remains as an anchor in the membrane's hydrophobic core whereas the surrounding DNA with its anionic nature is attracted towards the membrane by K^+ excess inside of the liposome resulting in a shorter inter-dye distance and an increased FRET. (d) Representative configuration of a simulated double membrane system, where two membrane patches separate two compartments filled with 150 mM KCl solution. A single dsDNA molecule is placed near one membrane to characterize effective interactions between the DNA and the membrane. A gradient of K^+ concentration is established by transferring four K^+ ions from one compartment to the other, corresponding to a drop of $\Delta\Psi=\pm1.3$ V. The local concentration of K^+ (e) and Cl^- (f) ions along the lipid bilayer is shown for the three ion gradient conditions. The z axis is defined in panel d. The profiles were averaged over 21 replica windows of the respective REUS MD simulations, each replica simulation being 120 ns long. The shaded region shows the location of the center of DNA in various windows. (g) Free energy ΔG of the 21 base pair dsDNA as a function of its *z*-coordinate for the three ion gradient conditions. The arrow implies the region shown in (d).

First, we are interested in three scenarios: a hyperpolarized, a neutral and a depolarized membrane with respect to the inner leaflet. We choose the hyperpolarization to be $\Delta\Psi=-100$ mV and the depolarization to be $\Delta\Psi=100$ mV, for which the buffer outside is exchanged with respect to the desired $\Delta\Psi$ and valinomycin is added before imaging. For all the samples, single Gaussian distributions are obtained and mean *PR* values of 0.593 ± 0.006 for $\Delta\Psi=-100$ mV, of 0.604 ± 0.005 for $\Delta\Psi=0$ mV and of 0.645 ± 0.003 for $\Delta\Psi=100$ mV are determined (Figure 2b and S5). When compared to the liposome-free sample, all the *PR* values are lower, which, in combination with the mono-Gaussian nature of the distributions, strongly suggests that the liposomes stayed intact throughout the experimental procedure. As the $\Delta\Psi=0$ mV sample shows an almost identical *PR* histogram as the control sample before the valinomycin addition, we are confident that all observed changes in the single-molecule fluorescence result from the $\Delta\Psi$ created and are not an interference with the ionophore (Figures 2b and S6). In contrast, there is a notable increase in the *PR* for the depolarized membrane compared to the hyperpolarized and neutral membrane which

bioRxiv preprint doi: https://doi.org/10.1101/2021.08.18.456762; this version posted August 18, 2021. The copyright holder for this preprint (which was not certified by peer review) is the author/funder. All rights reserved. No reuse allowed without permission.

implies that the DNA origami-based sensor is able to report transmembrane potentials on the single-molecule level.

The direction of FRET change implies that a more positive charge on the inside would attract the anionic donor dye-DNA hybrid towards the membrane so that FRET increases (see Figure 2c). An alternative mechanism, where the change of ion concentration outside the membranes modules the electrostatic force acting on the dye embedded in the lipid membrane is ruled out through a set of MD simulations that examined the distribution of the electrostatic potential in a double membrane system (Figure S7 and S8). It has been previously established that the electric potential of the membrane's interior is approximately 500 mV higher than the electric potential of the surrounding electrolyte.[35,36] A slight imbalance of ion concentration, i.e., a transfer of just one ion between the compartments of our simulated double membrane system as shown in Figure S7 produces the expected voltage difference between the electrolyte compartments. However, the gradient of the electrostatic potential across the leaflets of the lipid bilayers remains largely unaffected by the ion concentration gradient as most of the additional potential drop occurs at the interface of the lipid head groups and the electrolyte which is why we rule out a movement of the membrane-anchored ATTO647N.

To directly probe the effect of an ion concentration gradient on the interaction between DNA and a lipid membrane, we simulate another double membrane system (Figure 2d) where one DNA molecule is placed near the surface of one of the membranes parallel to the membrane surface. In addition to the system containing two charge-neutral electrolyte compartments (0 K^+), two variants of the system are created by moving four K^+ either to (4 K^+) or from (-4 K^+) the compartment containing the DNA, which corresponds to $\Delta\Psi$=0, $\Delta\Psi$=+1.3 and $\Delta\Psi$=-1.3 V, respectively (Figure S8). Such higher than experimental bias conditions are chosen to increase the effective force on dsDNA, facilitating convergence of the free-energy calculations (describe below). Replica exchange umbrella sampling (REUS) simulations[37] are performed for each system using 21 sampling windows (in 1 Å increments) for the distance between the centers of mass of the dsDNA and the nearby membrane along the *z*-axis. The resulting ion gradient

bioRxiv preprint doi: https://doi.org/10.1101/2021.08.18.456762; this version posted August 18, 2021. The copyright holder for this preprint (which was not certified by peer review) is the author/funder. All rights reserved. No reuse allowed without permission.

produces the expected ΔΨ across the compartments (Figure S8). Further, the local concentration of K^+ (Figure 2e) and Cl^- (Figure 2f) ions show a non-trivial behavior. In the profiles for all three samples, it is clearly visible that the K^+ concentration is increased close to the DNA whereas the Cl^- concentration is decreased which is due to the electrostatic attraction or repulsion to the anionic DNA backbone, respectively. In the case of an excess of K^+ ions inside (4 K^+), the K^+ concentration is also higher close to the inner leaflets. Interestingly, the concentration at the respective outer leaflets is reduced indicating a capacitive effect. The opposite behavior is observed for the lack of K^+ ions inside (-4 K^+). A complementary effect is observed for the Cl^- concentration (Figure 2f).

Further analysis of the REUS simulations yields the free energy of the dsDNA as a function of its proximity to the lipid membrane (Figure 2g). In the absence of a K^+ gradient, the free energy has a shallow minimum near the membrane surface, in agreement with our previous calculations.[38] Moving the positive charge across the membrane from the compartment housing (-4 K^+ trace), produces a free-energy minimum near the membrane surface promoting DNA attraction to the membrane surface. Moving the positive charge into the DNA compartment (4 K^+ trace) slightly increases repulsive interaction between DNA and the lipid membrane. These simulation results in qualitative agreement with our observation of a FRET increase for depolarized membranes and support the mechanism shown in Figure 2c.

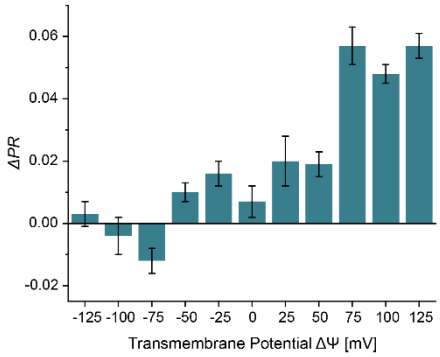

Figure 3. Changes *ΔPR* of the voltage sensor exposed to liposomes with different electrical transmembrane potentials ΔΨ. *ΔPR* is calculated by subtracting the mean *PR* before the potentials ΔΨ is created from the respective *PR* of the sample as indicated. The error bars represent the standard error of the mean after Gaussian error propagation. $N_{molecule}$=100 for each sample.

bioRxiv preprint doi: https://doi.org/10.1101/2021.08.18.456762; this version posted August 18, 2021. The copyright holder for this preprint (which was not certified by peer review) is the author/funder. All rights reserved. No reuse allowed without permission.

Next, we study the sensitivity of our voltage sensor in more detail and vary the potentials from ΔΨ=-125 mV to ΔΨ=125 mV in steps of 25 mV. For each sample the mean *PR* before creating ΔΨ is approximately the same (Figure S9). We therefore merge all reference data and define it as the mean of the control sample PR_{before}. This value is subtracted from the *PR* after ΔΨ is built up (Figure S5) as

$$\Delta PR = PR - PR_{before} \quad (3)$$

yielding the change *ΔPR*. The respective SEM is derived after Gaussian error propagation (see SI) and the data is presented in Figure 3. In accordance with the results discussed above, the *PR* value is only slightly increasing up to ΔΨ=50 mV and increases strongly in the range of 50 to 100 mV. The voltage sensor is thus able to transduce small changes in ΔΨ to single-molecule fluorescence signals. The non-linear response might indicate that the sensing unit above the membrane is not progressively shifting in the changing ΔΨ but that more specific conformational changes or displacements of the dyes are occurring.

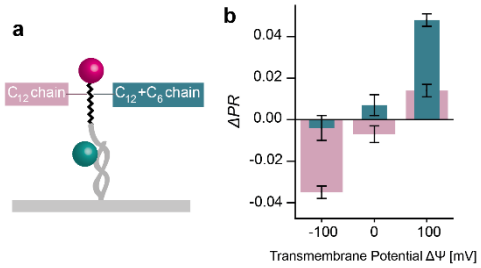

Figure 4. Changes *ΔPR* of the sensor with a C_{12} chain in the voltage-sensing unit as illustrated in (a) exposed to liposomes with ΔΨ=-100 mV, ΔΨ=0 mV and ΔΨ=100 mV (b, pink) in comparison to the voltage sensor with a C_{12}+C_6 chain (blue). *ΔPR* is estimated by subtraction of the mean *PR* before the potentials are created from the respective *PR* of the sample as indicated. The error bars represent the standard error of the mean after Gaussian error propagation. $N_{molecule}$ is ≥91 for each sample.

As our proposed mechanism is strongly relying on the relative positioning of the donor dye with respect to the acceptor dye, we check the sensitivity of the system for small changes of the linker. We therefor change the voltage-sensing unit minimally by shortening the carbon chain from a C_{12}+C_6 to a C_{12} chain eliminating also the additional phosphate group (Figure 4a, for details see Figure S2). Interestingly, in the

bioRxiv preprint doi: https://doi.org/10.1101/2021.08.18.456762; this version posted August 18, 2021. The copyright holder for this preprint (which was not certified by peer review) is the author/funder. All rights reserved. No reuse allowed without permission.

absence of the liposomes, the *PR* is only minimally higher for the shorter linker (*PR*=0.754 instead of 0.739). Upon binding to the liposome, however, the *PR* does only slightly decrease to *PR*=0.732 for the shorter linker indicating that stretching of the hydrophobic linker is mainly responsible for the FRET reduction in case of the C_{12}+C_6 linker (Figure S10 and S11). Varying ΔΨ of the liposomes exposed to the DNA origami voltage sensor with the shortened linker has an interesting effect on the measured *PR* values. Most of the signal change now occurs in the more physiologically relevant range between -100 mV and 0 mV whereas only a small *PR* increase is detected for positive ΔΨ (Figure 4b, S11 and S12). The direction of change is compatible with the idea that the FRET reduction is not a linear displacement in the ΔΨ but related to a more specific conformational change. As the DNA and the negatively charged dye are pulled towards the membrane by the shorter linker, it requires a more negative potential to displace them from the membrane so that the FRET reduction occurs.

CONCLUSION**.** Transmembrane potentials are key parameters to understand cellular functions and interactions and there is a great need for the development of smart sensing systems. We here present a DNA origami voltage sensor offering a robust platform to include many functionalities such as surface immobilization and liposome binding. It could be extended for further smart functionalities including specific cell or organelle recognition or for immune system camouflage.[39–41]

We also introduce a new sensing unit that is based on FRET between a hydrophobic dye that prefers location in the hydrophobic membrane core and a hydrophilic and anionic dye-DNA moiety that reacts with a *PR* change of ~5% for ΔΨ=100 mV. The DNA origami voltage sensors are studied by single-molecule spectroscopy on liposomes and the results are rationalized by MD simulations. While the fundamental working principle is implied by the experimental results, the MD simulations provide evidence that more specific interactions between the membrane and the sensing unit determine the sensitive voltage range that could be tuned by adaptation of the linker between donor and acceptor. Overall, our data show profound potential for this novel approach for ΔΨ sensors that could similarly be adapted for other sorts of sensors.

bioRxiv preprint doi: https://doi.org/10.1101/2021.08.18.456762; this version posted August 18, 2021. The copyright holder for this preprint (which was not certified by peer review) is the author/funder. All rights reserved. No reuse allowed without permission.

ASSOCIATED CONTENT

Supporting Information.

Supporting Information: Material and Methods, Illustration of DNA origami design in CaDNAno, DNA oligonucleotides used as staple strands for the DNA origami voltage sensor, Detailed sketch of the different voltage-sensor designs, Equilibrium MD simulation of dye conjugated dsDNA in aqueous and membrane anchored environment, Concentration of KCl and NaCl in the buffer inside and outside of the LUVs, Valinomycin bulk test, *PR* distributions for all samples of the C_{12}+C_6 sensor with transmembrane potentials $\Delta\Psi$, *PR* distributions of various C_{12}+C_6 samples compared, Voltage bias created by shuffling of a single ion in double membrane systems, Average electrostatic profile of the 0 K^+, 4 K^+ and -4 K^+ systems along the bilayer normal during the REUS MD simulations, *PR* distributions for all control samples of the C_{12}+C_6 sensor, *PR* distributions for all control samples of the C_{12} sensor, *PR* distributions for samples of the C_{12} sensor with transmembrane potentials $\Delta\Psi$ and without liposomes, *PR* distributions of various C_{12} samples compared, Captions to Supplementary Movies (docx)

Movie showing all-atom MD simulation of dyes on dsDNA (MP4)

Movie showing all-atom MD simulation of dyes on dsDNA with lipid membrane (MP4)

Movie showing mrDNA simulation of the DNA origami (MP4)

AUTHOR INFORMATION

Corresponding Author

* Philip Tinnefeld: philip.tinnefeld@cup.uni-muenchen.de

Funding Sources

bioRxiv preprint doi: https://doi.org/10.1101/2021.08.18.456762; this version posted August 18, 2021. The copyright holder for this preprint (which was not certified by peer review) is the author/funder. All rights reserved. No reuse allowed without permission.

DFG (grants INST 86/1904-1 FUGG, TI 329/10-1 and Project - ID 201269156 - SFB1032), National Science Foundation (USA) (DMR-1827346), XSEDE allocation grant (MCA05S028), Leadership Resource Allocation (MCB20012)

Notes

The authors declare no competing financial interest.

ACKNOWLEDGMENT

This work has been supported by the Deutsche Forschungsgemeinschaft DFG (grants INST 86/1904-1 FUGG, TI 329/10-1 and Project - ID 201269156 - SFB1032), and the National Science Foundation (USA) (DMR-1827346). We acknowledge the supercomputer time provided to A.A. and H.J. through the XSEDE allocation grant (MCA05S028) and the Leadership Resource Allocation (MCB20012) on Frontera at Texas Advanced Computing Center. A.A. and H.J. would like to thank Christopher Maffeo for his help in setting up the initial mrDNA simulation.

ABBREVIATIONS

GEVI, Genetically Encoded Voltage Indicator; FRET, Fluorescence Resonance Energy Transfer; ssDNA, single-stranded DNA; MD, Molecular Dynamic; TIRF, Total Internal Reflection Fluorescence; dsDNA, double-stranded DNA; smFRET, single-molecule FRET; ALEx, Alternating Laser Excitation; *PR*, *Proximity Ratio*; SEM, Standard Error of the Mean; REUS, Replica Exchange Umbrella Sampling.

References

(1) Sepehri Rad, M.; Choi, Y.; Cohen, L. B.; Baker, B. J.; Zhong, S.; Storace, D. A.; Braubach, O. R. Voltage and Calcium Imaging of Brain Activity. *Biophysical journal* **2017**, *113*, 2160–2167.

(2) Platisa, J.; Pieribone, V. A. Genetically encoded fluorescent voltage indicators: Are we there yet? *Current opinion in neurobiology* **2018**, *50*, 146–153.

(3) Adam, Y.; Kim, J. J.; Lou, S.; Zhao, Y.; Xie, M. E.; Brinks, D.; Wu, H.; Mostajo-Radji, M. A.; Kheifets, S.; Parot, V.*; et al.* Voltage imaging and optogenetics reveal behaviour-dependent changes in hippocampal dynamics. *Nature* **2019**, *569*, 413–417.

bioRxiv preprint doi: https://doi.org/10.1101/2021.08.18.456762; this version posted August 18, 2021. The copyright holder for this preprint (which was not certified by peer review) is the author/funder. All rights reserved. No reuse allowed without permission.

(4) Ma, Y.; Yamamoto, Y.; Nicovich, P. R.; Goyette, J.; Rossy, J.; Gooding, J. J.; Gaus, K. A FRET sensor enables quantitative measurements of membrane charges in live cells. *Nature biotechnology* **2017**, *35*, 363–370.

(5) Chanda, B.; Blunck, R.; Faria, L. C.; Schweizer, F. E.; Mody, I.; Bezanilla, F. A hybrid approach to measuring electrical activity in genetically specified neurons. *Nature neuroscience* **2005**, *8*, 1619–1626.

(6) Abdelfattah, A. S.; Kawashima, T.; Singh, A.; Novak, O.; Liu, H.; Shuai, Y.; Huang, Y.-C.; Campagnola, L.; Seeman, S. C.; Yu, J.*; et al.* Bright and photostable chemigenetic indicators for extended in vivo voltage imaging. *Science (New York, N.Y.)* **2019**, *365*, 699–704.

(7) Miller, E. W.; Lin, J. Y.; Frady, E. P.; Steinbach, P. A.; Kristan, W. B., JR; Tsien, R. Y. Optically monitoring voltage in neurons by photo-induced electron transfer through molecular wires. *Proceedings of the National Academy of Sciences of the United States of America* **2012**, *109*, 2114–2119.

(8) Nag, O. K.; Stewart, M. H.; Deschamps, J. R.; Susumu, K.; Oh, E.; Tsytsarev, V.; Tang, Q.; Efros, A. L.; Vaxenburg, R.; Black, B. J.*; et al.* Quantum Dot-Peptide-Fullerene Bioconjugates for Visualization of in Vitro and in Vivo Cellular Membrane Potential. *ACS nano* **2017**, *11*, 5598–5613.

(9) Park, K.; Kuo, Y.; Shvadchak, V.; Ingargiola, A.; Dai, X.; Hsiung, L.; Kim, W.; Zhou, H.; Zou, P.; Levine, A. J.*; et al.* Membrane insertion of-and membrane potential sensing by-semiconductor voltage nanosensors: Feasibility demonstration. *Science advances* **2018**, *4*, e1601453.

(10) Liu, J.; Zhang, R.; Shang, C.-F.; Zhang, Y.; Feng, Y.; Pan, L.; Xu, B.; Hyeon, T.; Bu, W.; Shi, J.*; et al.* Near-infrared voltage nanosensors enable real-time imaging of neuronal activities in mice and zebrafish. *Journal of the American Chemical Society* [Online early access]. DOI: 10.1021/jacs.0c01025.

(11) Klymchenko, A. S.; Stoeckel, H.; Takeda, K.; Mély, Y. Fluorescent probe based on intramolecular proton transfer for fast ratiometric measurement of cellular transmembrane potential. *The journal of physical chemistry. B* **2006**, *110*, 13624–13632.

(12) Nag, O. K.; Jeong, J.-E.; van Le, S.; Oh, E.; Woo, H. Y.; Delehanty, J. B. Anionic Conjugated Polyelectrolytes for FRET-based Imaging of Cellular Membrane Potential. *Photochemistry and photobiology* **2020**, *96*, 834–844.

(13) Saminathan, A.; Devany, J.; Veetil, A. T.; Suresh, B.; Pillai, K. S.; Schwake, M.; Krishnan, Y. A DNA-based voltmeter for organelles. *Nature nanotechnology* **2021**, *16*, 96–103.

(14) Rothemund, P. W. K. Folding DNA to create nanoscale shapes and patterns. *Nature* **2006**, *440*, 297–302.

(15) Douglas, S. M.; Dietz, H.; Liedl, T.; Högberg, B.; Graf, F.; Shih, W. M. Self-assembly of DNA into nanoscale three-dimensional shapes. *Nature* **2009**, *459*, 414–418.

(16) Douglas, S. M.; Marblestone, A. H.; Teerapittayanon, S.; Vazquez, A.; Church, G. M.; Shih, W. M. Rapid prototyping of 3D DNA-origami shapes with caDNAno. *Nucleic acids research* **2009**, *37*, 5001–5006.

(17) Shen, L.; Wang, P.; Ke, Y. DNA Nanotechnology-Based Biosensors and Therapeutics. *Advanced healthcare materials* **2021**, e2002205.

(18) Wei, R.; Martin, T. G.; Rant, U.; Dietz, H. DNA origami gatekeepers for solid-state nanopores. *Angewandte Chemie (International ed. in English)* **2012**, *51*, 4864–4867.

bioRxiv preprint doi: https://doi.org/10.1101/2021.08.18.456762; this version posted August 18, 2021. The copyright holder for this preprint (which was not certified by peer review) is the author/funder. All rights reserved. No reuse allowed without permission.

(19) Hernández-Ainsa, S.; Bell, N. A. W.; Thacker, V. V.; Göpfrich, K.; Misiunas, K.; Fuentes-Perez, M. E.; Moreno-Herrero, F.; Keyser, U. F. DNA origami nanopores for controlling DNA translocation. *ACS nano* **2013**, *7*, 6024–6030.

(20) Thomsen, R. P.; Malle, M. G.; Okholm, A. H.; Krishnan, S.; Bohr, S. S.-R.; Sørensen, R. S.; Ries, O.; Vogel, S.; Simmel, F. C.; Hatzakis, N. S.*; et al.* A large size-selective DNA nanopore with sensing applications. *Nature communications* **2019**, *10*, 5655.

(21) Jiang, Q.; Song, C.; Nangreave, J.; Liu, X.; Lin, L.; Qiu, D.; Wang, Z.-G.; Zou, G.; Liang, X.; Yan, H.*; et al.* DNA origami as a carrier for circumvention of drug resistance. *Journal of the American Chemical Society* **2012**, *134*, 13396–13403.

(22) Zhang, Q.; Jiang, Q.; Li, N.; Dai, L.; Liu, Q.; Song, L.; Wang, J.; Li, Y.; Tian, J.; Ding, B.*; et al.* DNA origami as an in vivo drug delivery vehicle for cancer therapy. *ACS nano* **2014**, *8*, 6633–6643.

(23) Nickels, P. C.; Wünsch, B.; Holzmeister, P.; Bae, W.; Kneer, L. M.; Grohmann, D.; Tinnefeld, P.; Liedl, T. Molecular force spectroscopy with a DNA origami-based nanoscopic force clamp. *Science (New York, N.Y.)* **2016**, *354*, 305–307.

(24) Kramm, K.; Schröder, T.; Gouge, J.; Vera, A. M.; Gupta, K.; Heiss, F. B.; Liedl, T.; Engel, C.; Berger, I.; Vannini, A.*; et al.* DNA origami-based single-molecule force spectroscopy elucidates RNA Polymerase III pre-initiation complex stability. *Nature communications* **2020**, *11*, 2828.

(25) Hemmig, E. A.; Fitzgerald, C.; Maffeo, C.; Hecker, L.; Ochmann, S. E.; Aksimentiev, A.; Tinnefeld, P.; Keyser, U. F. Optical Voltage Sensing Using DNA Origami. *Nano letters* **2018**, *18*, 1962–1971.

(26) Woo, S.; Rothemund, P. W. K. Programmable molecular recognition based on the geometry of DNA nanostructures. *Nature chemistry* **2011**, *3*, 620–627.

(27) Schmied, J. J.; Gietl, A.; Holzmeister, P.; Forthmann, C.; Steinhauer, C.; Dammeyer, T.; Tinnefeld, P. Fluorescence and super-resolution standards based on DNA origami. *Nature methods* **2012**, *9*, 1133–1134.

(28) Gietl, A.; Holzmeister, P.; Grohmann, D.; Tinnefeld, P. DNA origami as biocompatible surface to match single-molecule and ensemble experiments. *Nucleic acids research* **2012**, *40*, e110.

(29) Mobarak, E.; Javanainen, M.; Kulig, W.; Honigmann, A.; Sezgin, E.; Aho, N.; Eggeling, C.; Rog, T.; Vattulainen, I. How to minimize dye-induced perturbations while studying biomembrane structure and dynamics: PEG linkers as a rational alternative. *Biochimica et biophysica acta. Biomembranes* **2018**, *1860*, 2436–2445.

(30) Ha, T.; Enderle, T.; Ogletree, D. F.; Chemla, D. S.; Selvin, P. R.; Weiss, S. Probing the interaction between two single molecules: Fluorescence resonance energy transfer between a single donor and a single acceptor. *Proceedings of the National Academy of Sciences* **1996**, *93*, 6264–6268.

(31) Kapanidis, A. N.; Lee, N. K.; Laurence, T. A.; Doose, S.; Margeat, E.; Weiss, S. Fluorescence-aided molecule sorting: Analysis of structure and interactions by alternating-laser excitation of single molecules. *PNAS* **2004**, *101*, 8936–8941.

(32) Margeat, E.; Kapanidis, A. N.; Tinnefeld, P.; Wang, Y.; Mukhopadhyay, J.; Ebright, R. H.; Weiss, S. Direct observation of abortive initiation and promoter escape within single immobilized transcription complexes. *Biophysical journal* **2006**, *90*, 1419–1431.

bioRxiv preprint doi: https://doi.org/10.1101/2021.08.18.456762; this version posted August 18, 2021. The copyright holder for this preprint (which was not certified by peer review) is the author/funder. All rights reserved. No reuse allowed without permission.

(33) Preus, S.; Noer, S. L.; Hildebrandt, L. L.; Gudnason, D.; Birkedal, V. iSMS: Single-molecule FRET microscopy software. *Nat Methods* **2015**, *12*, 593–594.

(34) Hope, M. J.; Bally, M. B.; Webb, G.; Cullis, P. R. Production of large unilamellar vesicles by a rapid extrusion procedure. Characterization of size distribution, trapped volume and ability to maintain a membrane potential. *Biochimica et Biophysica Acta (BBA) - Biomembranes* **1985**, *812*, 55–65.

(35) Cheng, J.-X.; Pautot, S.; Weitz, D. A.; Xie, X. S. Ordering of water molecules between phospholipid bilayers visualized by coherent anti-Stokes Raman scattering microscopy. *PNAS* **2003**, *100*, 9826–9830.

(36) Aksimentiev, A.; Schulten, K. Imaging alpha-hemolysin with molecular dynamics: Ionic conductance, osmotic permeability, and the electrostatic potential map. *Biophysical journal* **2005**, *88*, 3745–3761.

(37) Sugita, Y.; Kitao, A.; Okamoto, Y. Multidimensional replica-exchange method for free-energy calculations. *The Journal of chemical physics* **2000**, *113*, 6042–6051.

(38) Morzy, D.; Rubio-Sánchez, R.; Joshi, H.; Aksimentiev, A.; Di Michele, L.; Keyser, U. F. Cations Regulate Membrane Attachment and Functionality of DNA Nanostructures. *Journal of the American Chemical Society* [Online early access]. DOI: 10.1021/jacs.1c00166. Published Online: May. 7, 2021.

(39) Douglas, S. M.; Bachelet, I.; Church, G. M. A logic-gated nanorobot for targeted transport of molecular payloads. *Science (New York, N.Y.)* **2012**, *335*, 831–834.

(40) Amir, Y.; Ben-Ishay, E.; Levner, D.; Ittah, S.; Abu-Horowitz, A.; Bachelet, I. Universal computing by DNA origami robots in a living animal. *Nature nanotechnology* **2014**, *9*, 353–357.

(41) Li, S.; Jiang, Q.; Liu, S.; Zhang, Y.; Tian, Y.; Song, C.; Wang, J.; Zou, Y.; Anderson, G. J.; Han, J.-Y.*; et al.* A DNA nanorobot functions as a cancer therapeutic in response to a molecular trigger in vivo. *Nature biotechnology* **2018**, *36*, 258–264.

bioRxiv preprint doi: https://doi.org/10.1101/2021.08.18.456762; this version posted August 18, 2021. The copyright holder for this preprint (which was not certified by peer review) is the author/funder. All rights reserved. No reuse allowed without permission.

SYNOPSIS

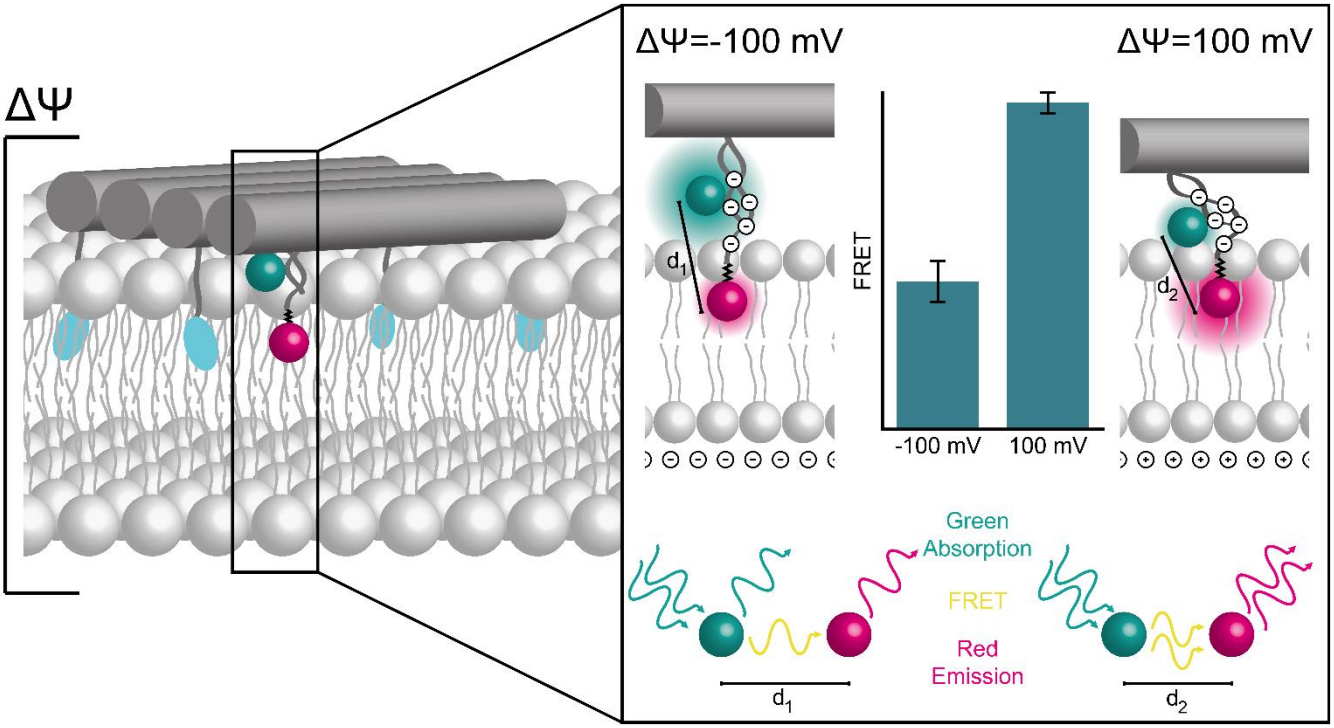

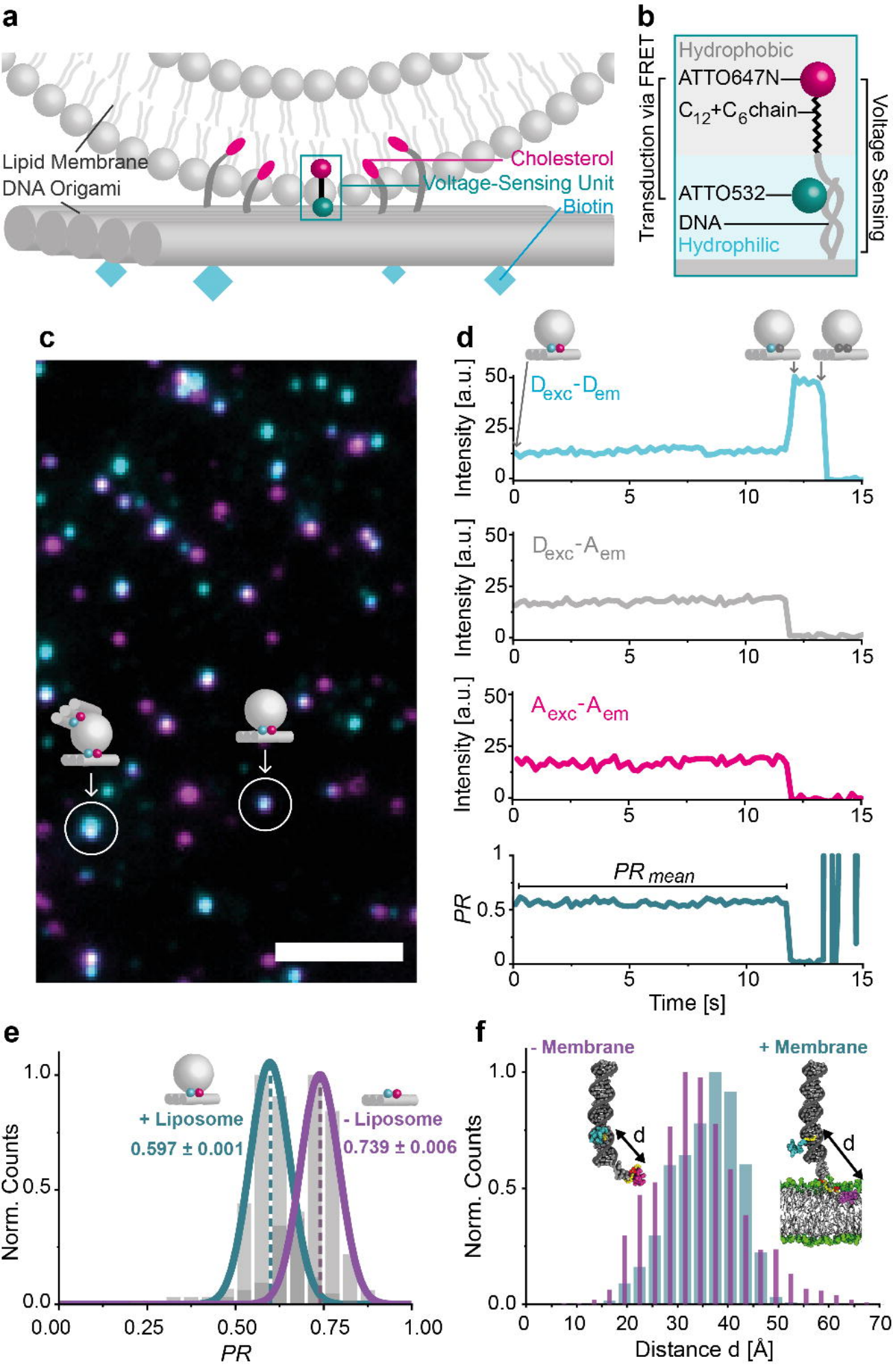
a
Lipid Membrane
DNA Origami
Cholesterol
Voltage-Sensing Unit
Biotin
b
Hydrophobic
ATTO647N
C12+C6chain
ATTO532
DNA
Hydrophilic
Transduction via FRET
Voltage Sensing
c
d
Dexc-Dem
Dexc-Aem
Aexc-Aem
PR mean
Intensity [a.u.]
PR
Time [s]
e
+ Liposome
0.597 ± 0.001
- Liposome
0.739 ± 0.006
Norm. Counts
PR
f
- Membrane
+ Membrane
d
Norm. Counts
Distance d [Å]

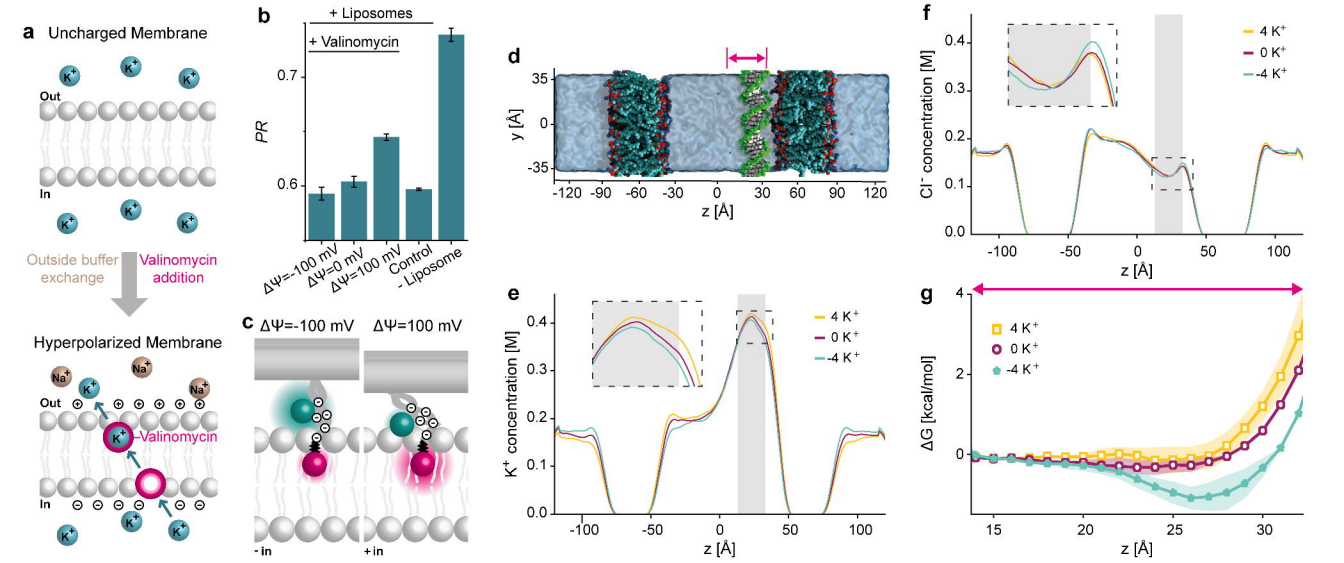
a
Uncharged Membrane
Out
In
Outside buffer exchange
Valinomycin addition
Hyperpolarized Membrane
Valinomycin
b
+ Liposomes
+ Valinomycin
PR
0.7
0.6
ΔΨ=-100 mV
ΔΨ=0 mV
ΔΨ=100 mV
Control - Liposome
c
ΔΨ=-100 mV
ΔΨ=100 mV
- in
+ in
d
y [Å]
z [Å]
e
K+ concentration [M]
4 K+
0 K+
-4 K+
z [Å]
f
Cl- concentration [M]
4 K+
0 K+
-4 K+
z [Å]
g
ΔG [kcal/mol]
4 K+
0 K+
-4 K+
z [Å]

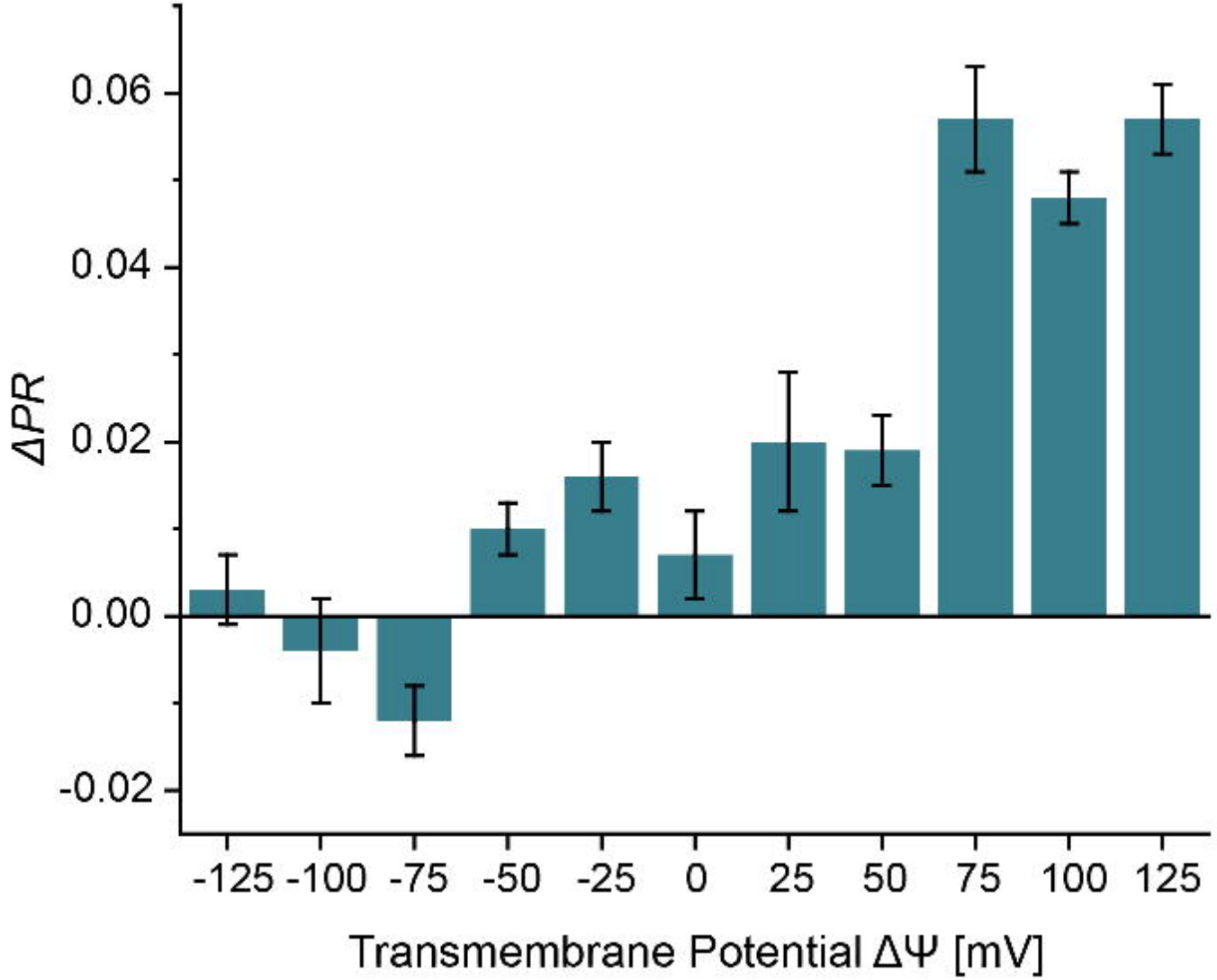
0.06
0.04
0.02
0.00
-0.02
ΔPR
-125
-100
-75
-50
-25
0
25
50
75
100
125
Transmembrane Potential ΔΨ [mV]

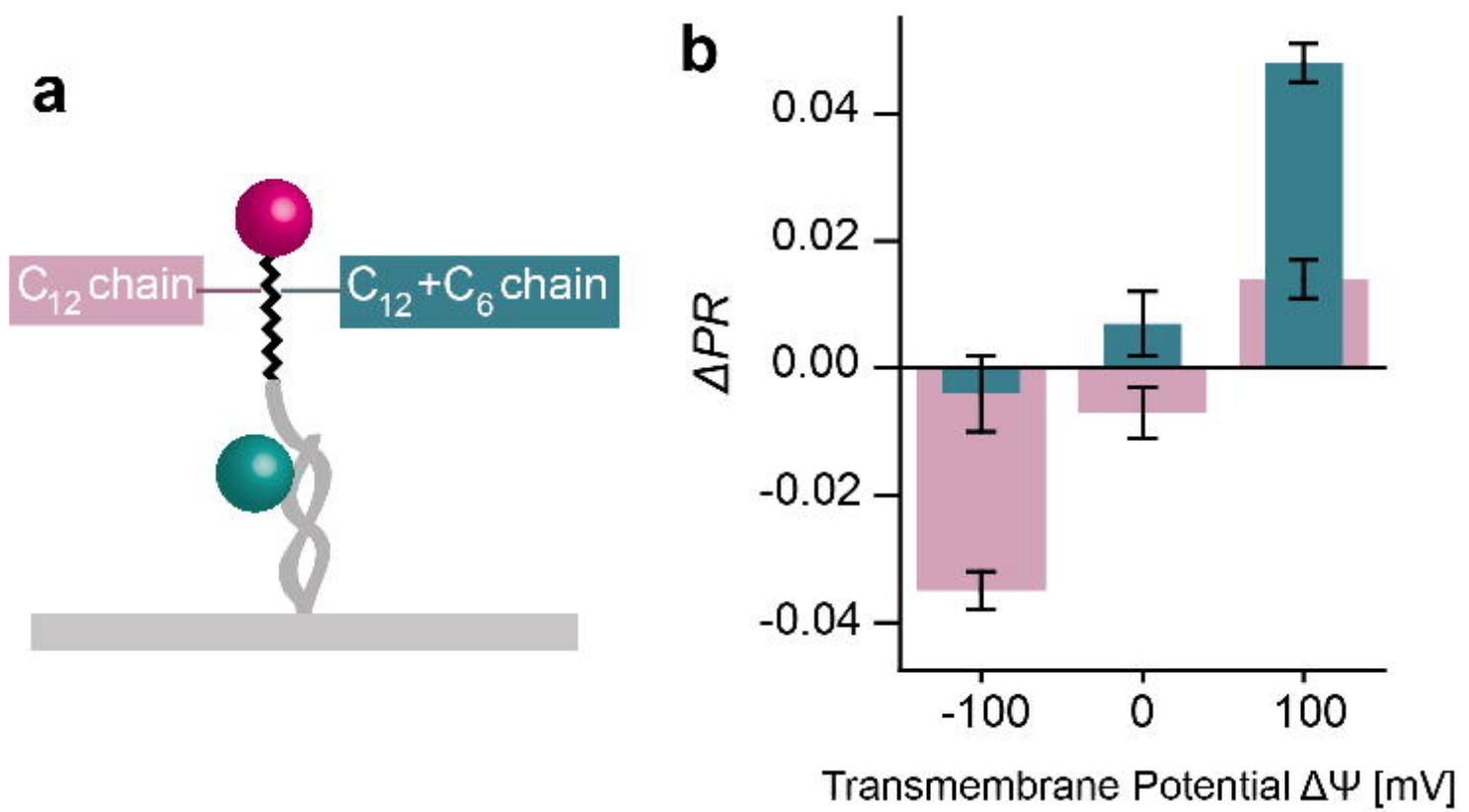
a
C12 chain
C12+C6 chain
b
0.04
0.02
0.00
-0.02
-0.04
ΔPR
-100
0
100
Transmembrane Potential ΔΨ [mV]